CHEMISTRY OF MATERIALS
Article

Chem. Mater. **2009,** *21,* 5617–5626 5617
DOI:10.1021/cm902230u

Molecular Precursors for CdS Nanoparticles: Synthesis and Characterization of Carboxylate−Thiourea or −Thiosemicarbazide Cadmium Complexes and Their Decomposition

Trinanjana Mandal,[†] Vitalie Stavila,[†] Irene Rusakova,[‡] Saunab Ghosh,[†] and Kenton H. Whitmire*,[†]

[†]*Department of Chemistry, MS-60, Rice University, 6100 Main Street, Houston, Texas 77005 and* [‡]*Texas Center for Superconductivity at the University of Houston (TcSUH), HSC Building, University of Houston, Texas 77204-5002*

Received July 21, 2009. Revised Manuscript Received October 21, 2009

The reactions of cadmium acetate with picolinic (Hpic), 2,6-dipicolinic (H_2pydc), or salicylic acid (H_2sal) followed by the addition of thiourea (tu) or thiosemicarbazide (ths) yielded six new coordination complexes, including $[Cd(Hsal)_2(tu)_2]$ (**1a**), $[Cd(pic)_2(tu)_2]\cdot 0.5H_2O$ (**2a**), $[Cd(pic)_2(ths)_2]\cdot 2H_2O$ (**2b**), $[Cd(pydc)(tu)_2]$ (**3a**), and $[Cd(pydc)(ths)_2(H_2O)]\cdot 2H_2O$ (**3b**). All of the compounds were characterized spectroscopically and by elemental analysis. Compounds **1a**, **2a**, **2b**, **3a**, and **3b** formed well-defined crystals and were further characterized by single-crystal X-ray diffraction. Additionally, reaction of $Cd(Hsal)_2$ with ths produced a compound **1b** of uncertain composition that had bound ths as evidenced by ESI-MS. The most likely formula for this compound was $Cd(sal)(ths)_x$, but $Cd(Hsal)_2(ths)_x$ was also possible. In compounds **1a** and **3a**, the Cd(II) ion exhibits penta-coordinated geometry; in **1a**, three carboxylate oxygen atoms and two sulfur atoms from thiourea complete the coordination sphere, whereas in **3a**, two carboxylate oxygen atoms, one pyridyl nitrogen atom and two sulfur atoms from thiourea are within the coordination sphere. In **2a** and **2b**, the Cd(II) ions are hexa-coordinated, binding to two carboxyl oxygen atoms, two pyridyl nitrogen atoms, and two sulfur atoms in both cases. In **3b**, the thiosemicarbazide acts as a chelating ligand, coordinating through both the sulfur atom and the primary nitrogen atom of $NHNH_2$ group. In addition, two carboxylate oxygen atoms, one pyridyl nitrogen atom, and one water molecule are within the coordination sphere making the central Cd(II) ion hepta-coordinated. Although the complexes appeared to be slightly photosensitive they are stable under ambient conditions. The precursors were decomposed at 175 °C using N-cetyl trimethylammonium bromide, ethylenediamine, oleylamine, or hexadecylamine as surfactants. The CdS nanoparticles were explored by scanning electron microscopy (SEM), transmission electron microscopy (TEM), thermogravimetric analysis (TGA), X-ray powder diffraction (XRPD), and energy-dispersive spectroscopy (EDS). Solvothermal decompositions using CTAB in an aqueous solution gave rise to microsized flowerlike crystals; long-chain organic amines such as oleylamine or hexadecylamine led to spherical or ellipsoidal nanoparticles, ethylenediamine produced nanorods, and a mixed surfactant of tri-n-octylphosphine and oleylamine produced multipod structures. TEM studies revealed planar defects (such as polysynthetic and multiplet twinning) in the nanocrystals, which gives an explanation for mechanism of growth. Interestingly, linear arms that arise from polypodal branching may not necessarily be a single phase. Even straight arms may exhibit highly regular polysynthetic twinning. From XRPD studies, it was found that most of the nanostructures were of the stable hexagonal phase. However, in two cases, the nanostructures were found to be predominantly of a metastable orthorhombic phase. Variation of precursor slightly affected the morphology of the decomposition product.

Introduction

Synthesis of inorganic semiconductor nanoparticles (NPs) is of major interest because of their shape- and size-dependent optical and electronic properties, as well as their potential applications in the fields of nonlinear optics, light-emitting devices, and biological diagnostics. One of the major challenges in this field is the controllable synthesis of NPs with uniform shapes and sizes. As CdS is one of the most important group II−VI semiconductors, various methods have been developed to control shapes and sizes in this system on the nanoscale over the past few years. These methods include hard templates (such as aluminum oxide membranes), soft templates (such as liquid crystals,[1] micelles,[2] polymers[3]), structure-directing

*To whom correspondence should be addressed. E-mail: whitmir@rice.edu. Phone: (713) 348-5650. Fax: (713) 348-5155.

(1) Tura, C.; Coombs, N.; Dag, O. *Chem. Mater.* **2005**, *17*, 573.
(2) Xu, W.; Akins, D. L. *Mater. Lett.* **2004**, *58*, 2623.
(3) Zhang, Y.; Chen, Y.; Niu, H.; Gao, M. *Small* **2006**, *2*, 1314.

Published on Web 11/12/2009

coordinating solvents, vapor liquid solid (VLS) methods, etc. We have been exploring the effect of single-source molecular precursors on the morphology and size of the nanoparticles synthesized. The use of a single-source precursor can control the metal stoichiometry in the final product, similar to complexes used for MOCVD.[4,5] Molecular precursors also help achieve a homogeneous distribution of metal ion in the final product as a result of the intimate mixing on the molecular level.[5−7] Furthermore, the bridging or chelating organic ligands present in these complexes prevent molecular segregation and the loss of volatile organic moieties may impart desirable structural features in the end product such as high surface area, low density, connected channels, or the formation of metastable phases.[8−10]

Several complexes of Cd with sulfur-containing ligands have been used as precursors to synthesize CdS NPs. Dithiocarbamato complexes [$Cd(S_2CNR_2)_2$] have been well-studied,[11,12] and O'Brien and co-workers have reported the use of Cd complexes of ethylxanthate,[13] thiohydrocarbazide[14] and alkyl-substituted thiourea[15] as precursors. In the latter case, CdS nanorods are produced in a coordinating solvent such as tri-n-octylphosphine oxide (TOPO). CdS NPs have also been synthesized by thermolysis of Cd(II) N,N′-bis(thiocarbamoyl)hydrazide,[16] and Liu et al. used a Cd(II) O,O′-dialkyldithiophosphate.[17] The precursors examined to date are designed for use under nonaqueous conditions, and additional thio-containing molecules are often needed to assist in precursor decomposition. We have explored the synthesis of CdS precursors that can be used in both aqueous and nonaqueous solvent, ideally without the need for additional sulfur containing molecules. To synthesize the precursor complexes, salicylic, picolinic, and 2,6-dipicolinic acids were natural choices as they can coordinate as a multidentate ligands that produce stable metal complexes. As a sulfur source, thiourea and thiosemicarbazide were chosen, as they are readily available and inexpensive starting materials.

We have also investigated the mechanism of formation of CdS NPs of variable shapes and sizes under the employed reaction conditions. Special attention was given toward understanding the growth mechanism of branched nanostructures. A considerable amount of effort has been directed toward II−VI semiconductors such as (ZnO, ZnSe, CdTe, etc.) There are two different hypotheses for the growth of polypodal structures. One proposal postulates that it is an effect of wurtzite-zinc blende polytypism, where the stacking defects in the initial cubic (zinc blende) nucleus initiates the growth of hexagonal (wurtzite) arms from four equivalent facets.[11,18−21]

An alternate hypothesis is that the initial nucleus has eight wurtzite domains connected to each other by multiple-twinned boundaries. Among these eight domains, four are slow growing and four are fast growing hence the tetrapod shape develops. Some studies on the growth of CdTe, ZnO, and ZnSe tetrapods support the latter mechanism.[22−27] In this article, we report the synthesis and characterization of six cadmium(II) carboxylate-thiourea or thiosemicarbazide mixed ligand complexes, their decomposition to crystalline CdS NPs, and provide data on the mechanism of growth of NPs.

Experimental Section

Materials. Cadmium acetate dihydrate (98%), thiosemicarbazide (99%), thiourea (99%), picolinic acid (99%), 2,6-dipicolinic acid (99%), cetyltrimethylammonium bromide (CTAB; technical grade), tri-n-octylamine (TOA; 98%), hexadecylamine (HDA), 1-dodecanethiol (DDT) (98%), and trioctylphosphine (TOP; technical grade 90%) were obtained from Sigma-Aldrich. Trioctylphosphine oxide (TOPO; 90%) was bought from Strem chemicals. Salicylic acid and ethylenediamine were bought from Fischer Scientific. All the chemicals were used without further purification. All the solvents were distilled using standard procedures.[28]

Characterization Details. NMR spectra were recorded on a Bruker Avance-400 MHz NMR spectrometer. Infrared data were recorded on a Nicolet 670 FT-IR spectrometer using attenuated total reflectance. Elemental analyses were performed at the Galbraith Laboratories.Powder X-ray diffraction (XRPD) data were obtained with a Rigaku D/Max-2100PC diffractometer operating with unfiltered Cu Kα radiation

(4) Kelly, A. T.; Rusakova, I.; Ould-Ely, T.; Hofmann, C.; Luettge, A.; Whitmire, K. H. *Nano Lett*. **2007**, *7*, 2920.
(5) Thurston, J. H.; Ely, T. O.; Trahan, D.; Whitmire, K. H. *Chem. Mater*. **2003**, *15*, 4407.
(6) Pohl, I. A. M.; Westin, L. G.; Kritikos, M. *Chem.—Eur. J*. **2001**, *7*, 3438.
(7) Thurston John, H.; Whitmire, K., H. *Inorg. Chem*. **2003**, *42*, 2014.
(8) Boulmaaz, S.; Papiernik, R.; Hubert-Pfalzgraf, L. G.; Septe, B.; Vaissermann, J. *J. Mater. Chem* **1997**, *7*, 2053.
(9) Chen, X.; Wang, Z.; Wang, X.; Wan, J.; Liu, J.; Qian, Y. *Chem. Lett*. **2004**, *33*, 1294.
(10) Liu, W. *Mater. Lett*. **2006**, *60*, 551.
(11) Jun, Y. W.; Lee, S. M.; Kang, N. J.; Cheon, J. *J. Am. Chem. Soc*. **2001**, *123*, 5150.
(12) Memon, A. A.; Afzaal, M.; Malik, M. A.; Nguyen, C. Q.; O'Brien, P.; Raftery, J. *J. Chem. Soc., Dalton Trans*. **2006**, 4499.
(13) Nair, P. S.; Radhakrishnan, T.; Revaprasadu, N.; Kolawole, G.; O'Brien, P. *J. Mater. Chem*. **2002**, *12*, 2722.
(14) Nair, P. S.; Radhakrishnan, T.; Revaprasadu, N.; Kolawole, G. A.; O'Brien, P. *Polyhedron* **2003**, *22*, 3129.
(15) Nair, P. S.; Chili, M. M.; Radhakrishnan, T.; Revaprasadu, N.; Christian, P.; O'Brien, P. *S. Afr. J. Sci*. **2005**, *101*, 466.
(16) Sreekumari Nair, P.; Revaprasadu, N.; Radhakrishnan, T.; Kolawole, G. A. *J. Mater. Chem*. **2001**, *11*, 1555.
(17) Shen, X.; Shi, X.; Kang, B.; Liu, Y.; Gu, L.; Huang, X. *J. Coord. Chem*. **1999**, *47*, 1.
(18) Chen, M.; Xie, Y.; Lu, J.; Xiong, Y.; Zhang, S.; Qian, Y.; Liu, X. *J. Mater. Chem* **2002**, *12*, 748.
(19) Manna, L.; Milliron, D. J.; Meisel, A.; Scher, E. C.; Alivisatos, A. P. *Nat. Mater*. **2003**, *2*, 382.
(20) Manna, L.; Scher, E. C.; Alivisatos, A. P. *J. Am. Chem. Soc*. **2000**, *122*, 12700.
(21) Yu, W. W.; Wang, Y. A.; Peng, X. *Chem. Mater*. **2003**, *15*, 4300.
(22) Carbone, L.; Kudera, S.; Carlino, E.; Parak, W. J.; Giannini, C.; Cingolani, R.; Manna, L. *J. Am. Chem. Soc*. **2006**, *128*, 748.
(23) Dai, Y.; Zhang, Y.; Wang, Z. L. *Solid State Commun*. **2003**, *126*, 629.
(24) Iwanaga, H.; Fujii, M.; Ichihara, M.; Takeuchi, S. *J. Cryst. Growth* **1994**, *141*, 234.
(25) Iwanaga, H.; Fujii, M.; Takeuchi, S. *J. Cryst. Growth* **1993**, *134*, 275.
(26) Iwanaga, H.; Fujii, M.; Takeuchi, S. *J. Cryst. Growth* **1998**, *183*, 190.
(27) Nishio, K.; Isshiki, T.; Kitano, M.; Shiojiri, M. *Phys. Condens. Matter*. **1997**, *76*, 889.
(28) Armarego, W. L. F.; Chai, C., *Purification of Laboratory Chemicals*, 5th ed.; Elsevier: Amsterdam, 2003.

(λ = 1.5406 Å) at 40 kV and 40 mA. The contribution from $K\alpha_2$ radiation was removed using the Rachinger algorithm. Goniometer alignment was verified by daily analysis of a Rigaku-supplied SiO_2 reference standard. The processing of the powder diffraction results and phase identification was accomplished using the program JADE.[29] TGA studies were performed on a Sieko DT/TGA 200 instrument in alumina pans under an argon-containing atmosphere. Approximately 20 mg of the sample to be studied was placed in an alumina pan in the furnace of a Sieko TGA/DTA Instruments. The sample was heated to 400 °C at a rate of 10 °C/min. Transmission electron microscopy (TEM) experiments were performed by depositing a drop of suspension diluted in hexane on a carbon coated copper grid. The solvent was evaporated and the sample was analyzed using JEOL 2000FX and JEOL 2010 microscopes that were equipped with energy dispersive spectrometers. Conventional and high-resolution TEM imaging, selected area electron diffraction (SAED) and energy-dispersive spectroscopy (EDS) methods have been used for analysis of the cadmium sulfide NPs. Precautions have been taken to prevent structural changes in the studied material caused by heating effects of the electron beam. The ESI-MS data were obtained on an MS micrOTOF ESI mass spectrometer.

The optical absorption spectra of the samples were measured on a double-beam UV−visible spectrometer; Cary 400 (400 to 900 nm, 1 nm step) using a 4 mm × 10 cm quartz fluorimeter cell (Starna Cells). Photoluminescence emission studies were performed using a Spex Fluorolog 3-211(J-Y Horiba) spectrofluorometer equipped with a photomultiplier tube (PMT) for visible emission detection in a similar cuvette. Typical slit widths were 3 × 3 nm in excitation and emission using with 2 nm step.

Synthesis of $[Cd(Hsal)_2(tu)_2]$, 1a. $Cd(OAc)_2 \cdot 2H_2O$ (267 mg, 1.00 mmol) and H_2Sal (276 mg, 2.00 mmol) were dissolved in a 100 mL beaker in 50-mL water and stirred at reflux until the volume of the solution was reduced to ~ 20 mL. Thiourea (160 mg, 2.10 mmol) dissolved in 10 mL of water was added slowly, and the clear solution was stirred for 30 min. The solution was left at room temperature for crystallization. Crystals of **1a** formed after about 24 h, and were washed with hexane and dried in vacuum. Yield, ~350 mg (65%) ^{1}H NMR (DMSO-d^6): 6.77 (m, ArH), 7.34 (m, ArH), 7.80 (m, ArH), 7.82 (m, ArH), 3.43 (s, br), ^{13}C NMR (DMSO-d^6): 116.51 (ArC), 117.82 (ArC), 119.50 (ArC), 130.22 (ArC), 133.25 (ArC), 161.12 (*C*OH), 173.82 (*C*O_2), 183.70 (*C*S$(NH_2)_2$). Elemental anal. found (calcd) for $C_{16}H_{18}CdO_6N_4S_2$: C, 35.54 (35.66); H, 3.28 (3.36). Decomposes at 174 °C before melting.

Synthesis of 1b. A similar procedure as described for **1a** was employed, using 184 mg (2.02 mmol) of thiosemicarbazide instead of thiourea. Yield ~290 mg (55%, yield calculated using molecular formula [Cd(sal)(ths)$_3$], see discussion). ^{1}H NMR (DMSO-d^6): 6.77 (m, ArH), 7.27 (m, ArH), 7.76 (m, ArH), 8.1 (m, ArH), 4.03 (m, br),^{13}C NMR (DMSO-d^6): 116.38 (ArC), 117.55 (ArC), 119.51 (ArC), 130.18 (ArC), 132.58 (ArC), 161.33 (*C*OH), 173.53 (*C*O_2), 181.05 (*C*SNH_2NHNH_2).

Synthesis of $[Cd(pic)_2(tu)_2] \cdot 0.5H_2O$, 2a. An aqueous solution (650 mL) of $Cd(OAc)_2 \cdot 2H_2O$ (533 mg, 2.00 mmol) and picolinic acid (492 mg, 4.00 mmol) was stirred at 100 °C in a beaker until the volume of the solution was reduced to ~100 mL. An aqueous solution of thiourea (308 mg, 4.04 mmol) was added and the resulting clear solution was left for crystallization for 24 h to produce colorless crystals. The product was washed with diethyl ether to give ~785 mg (76%) of the compound. Additional product was obtained after concentration of the filtrate. ^{1}H NMR (DMSO-d^6): 7.06 (s, broad, H of thiourea), 7.15 (m, ArH), 7.70 (m, ArH), 8.00 (m, ArH), 8.77 (m, ArH). ^{13}C NMR (DMSO-d^6): 125.91 (ArC), 126.51 (ArC), 139.18 (ArC), 133.25 (ArC), 146.96 (ArC), 151.92 (*C*COOH), 169.74 (*C*O_2) 183.76 (*C*S$(NH_2)_2$). Elemental anal. found (calcd) for $C_{28}H_{34}Cd_2O_9N_{12}S_4$: C, 32.39 (32.44); H, 3.22 (3.28) Melting point: 215 °C .

Synthesis of $[Cd(pic)_2(ths)_2] \cdot 2H_2O$, 2b. $Cd(OAc)_2 \cdot 2H_2O$ (266 mg, 1.00 mmol) and picolinic acid (246 mg, 2.00 mmol) were dissolved in 200 mL of water and the resulting solution was stirred at 100 °C in a beaker until the volume of the solution was reduced to ~10 mL. Solid thiosemicarbazide (184 mg, 2.02 mmol) was added to the hot solution of cadmium(II) picolinate and the resulting clear solution was left to cool for 2 days to yield colorless crystals. Yield ~500 mg (87%). ^{1}H NMR (DMSO d^6): 7.06 (s, broad, H of thiourea), 7.15 (m, ArH), 7.70 (m, ArH), 8.00 (m, ArH), 8.77(m, ArH). ^{13}C NMR (DMSO-d^6): 125.95 (ArC), 126.45 (ArC), 139.22 (ArC), 146.74 (ArC), 151.87 (*C*COOH), 169.49 (*C*O_2) 181.14 (*C*SNH_2NHNH_2). Elemental anal. found (calcd) for $C_{14}H_{22}CdO_6N_8S_2$: C, 25.01 (29.22); H, 4.18 (3.82). Melting point: 108 °C. The compound is slightly photosensitive, which has made it difficult to get better elemental analyses.

Synthesis of $[Cd(pydc)(tu)_2]$, 3a. $Cd(OAc)_2 \cdot 3H_2O$ (532 mg, 2.00 mmol) was dissolved upon heating in 10 mL of ethanol/water 1:1 (by volume). A solution of thiourea (602 mg, 8.00 mmol) in 30 mL of 1:1 ethanol/water was added and the mixture was stirred for 30 min, followed by the addition of 2,6-pyridinedicarboxylic acid (415 mg, 2.00 mmol) in 20 mL of warm water. The mixture was allowed to stir, resulting in precipitation of a microcrystalline white compound, which was washed with water and ethanol and then dried in vacuum. Yield ~790 mg, 92%. ^{1}H NMR (DMSO-d^6): 8.233 (m, ArH), 7.6 (br, m, H of th), ^{13}C NMR (DMSO-d^6): 165.49(*C*O_2), 149.22 (*C*COOH), 141.69 (ArC), 125.33 (ArC), 181.66 (*C*S$(NH_2)_2$). Elemental anal. found (calcd) for $C_9H_{11}CdO_4N_5S_2$: C, 25.10 (25.13); H, 2.43 (2.55). Melting point: 255 °C.

Synthesis of $[Cd(pydc)(ths)_2(H_2O)] \cdot 2H_2O$, 3b. This compound was prepared as described for **1a**, using 729 mg (8.00 mmol) of thiosemicarbazide instead of thiourea. Yield ~925 mg (90%). ^{1}H NMR (DMSO-d^6): 8.645 (s, ArH), 8.162 (s, ArH), 7.194 (br, m, H of ths). Elemental anal. found (calcd) for $C_9H_{15}CdO_7N_7S_2$: C, 21.59 (21.01); H, 3.45 (2.91). Decomposes at 195 °C before melting.

Single-Crystal X-ray Structural Determinations. X-ray crystallographic data for the precursors are given in Table 1. The data for **1a**, **2a**, **2b**, **3a**, and **3b** were collected at 298 K on a Bruker SMART 1000 CCD diffractometer equipped with a Mo-target X-ray tube in a hemisphere with 10 or 15 s exposure times.[30] The frames were integrated with the Bruker SAINT software package[31] and corrected for absorption effects using empirical method (SADABS).[32] The structures were solved using direct methods and refined by full-matrix least-squares on F^2 using the Bruker SHELXL software package.[33] The coordinates of cadmium and sulfur atoms were found using direct methods. The remaining atoms were located in subsequent least-squares difference Fourier cycles. Hydrogen atoms

(29) *Jade, XRD Pattern-Processing for the PC*, version 2.1; MDI: Livermore, CA, 1994.

(30) *SMART*, version 5.04; Bruker AXS Inc.: Madison, WI, 2002.
(31) *SAINT*, version 7.23a; Bruker AXS Inc.: Madison, WI, 2002.
(32) Sheldrick, G. *SADABS*, version 5.1; University of Göttingen: Göttingen, Germany, 1997.
(33) Sheldrick, G. *SHELXTL*, University of Göttingen: Göttingen, Germany, 2001.

Table 1. Selected Bond Lengths (Å) for 1a, 2a, 2b, 3a, and 3b

bond type	1a	2a	2b	3a	3b
Cd(1)−S(1)	2.558(9)	2.6066(9)	2.6066(9)	2.518(2)	2.740(1)
Cd(1)−S(2)	2.579(9)	2.6266(7)	2.6266(7)	2.511(2)	2.616(1)
Cd(1)−O(1)					2.402(2)
Cd(1)−O(11)	2.468(19)	2.372(1)	2.372(1)	2.398(3)	2.425(2)
Cd(1)−O(12)	2.348(2)				
Cd(1)−O(13)				2.407(3)	2.500(2)
Cd(1)−O(21)	2.2332(19)	2.323(1)	2.323 (1)		
Cd(1)···O(22)	2.8103(20)				
Cd(1)−N(1)		2.383(2)	2.383(2)	2.264(3)	2.318(2)
Cd(1)−N(2)		2.353(2)	2.353(2)		
Cd(1)−N(23)					2.402(3)

were included in idealized positions. Anisotropic displacement parameters were assigned to all non-hydrogen atoms.

General Methods in the Synthesis of CdS NPs. Two general decomposition techniques were followed, (1) standard Schlenk technique and (2) solvothermal decomposition using Teflon-lined stainless steel reactor. For the Schlenk reactions a 100-mL 3-neck flask was fitted with a reflux condenser and the desired amount of the appropriate precursor were added followed by the required volume of surfactant solution. The flask was placed under a vacuum and purged with argon three times while stirring rapidly. The reaction mixture was then stirred vigorously while the temperature was ramped up to either 120 or 175 °C and maintained at that temperature for varied amounts of time. In a typical solvothermal decomposition, a measured amount of the precursor was mixed with the surfactant solution. The mixture was sealed in a 23 mL Teflon lined stainless steel reactor and then heated at either 120 or 175 °C for 16 h. After cooling to room temperature, the yellow to orange precipitate of CdS was collected and washed by centrifugation with water and ethanol.

Decomposition of 1a and 2b in the Presence of CTAB. 200 mg of precursor **1a** or 100 mg of **2b** were mixed with 200 mg of CTAB and 15 mL of water with stirring for 30 min, and the mixture was heated in a Teflon-lined stainless steel Parr bomb for 16 h at 175 °C. The autoclave was then cooled to room temperature, and the products were collected and washed repeatedly in water and ethanol.

Decomposition of 1a in Ethylenediamine or Oleylamine. 200 mg of precursor **1a** was stirred with 15 mL of ethylenediamine for 30 min and then the mixture was heated in a Teflon-lined stainless steel Parr bomb for 16 h at 175 °C. It was then allowed to cool to room temperature. The collected orange-yellow precipitate was washed repeatedly in water and ethanol.

Decomposition of 1a or 2b in Oleylamine. Two hundred milligrams of the precursor **1a** or **2b** was dissolved in 12 mL of oleylamine, and the mixture was heated at 120 °C for 16 h in a Teflon-lined stainless steel Parr bomb. Next, the reaction mixture was allowed to cool to room temperature. The solid was collected and washed with ethanol and water.

Decomposition of 1b in Oleylamine with Added Hydrochloric Acid and TOPO. 200 mg of precursor **1b** was dissolved in 8 mL of oleylamine, after which 0.1 mL of dilute HCl and 1 g of TOPO were added to the mixture; it was then heated to 120 °C in a Teflon-lined stainless steel Parr bomb for 16 h. Next, the reaction mixture was allowed to cool to room temperature. The solid was collected and washed with ethanol and water.

Decomposition of 1b in Oleylamine with the Presence of TOP. 200 mg of the precursor **1b** was mixed with 8 mL of oleylamine and 1 g of TOP. The mixture was heated at 120 °C for 16 h and allowed to cool to room temperature. The yellow-orange precipitate was washed with water and ethanol and collected by centrifugation.

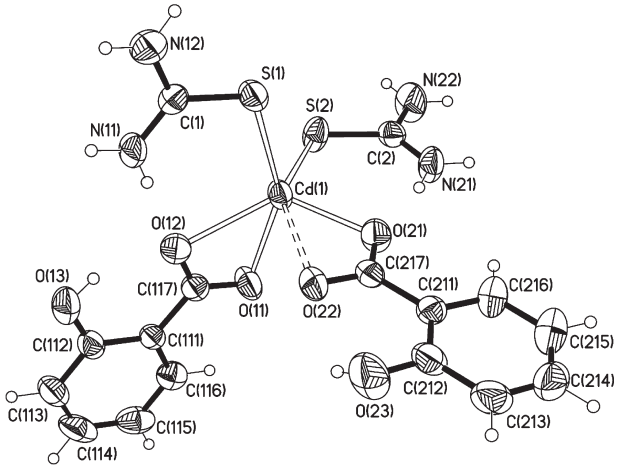

Figure 1. X-ray crystallographic structure of **1a** with thermal ellipsoids at the 40% probability level.

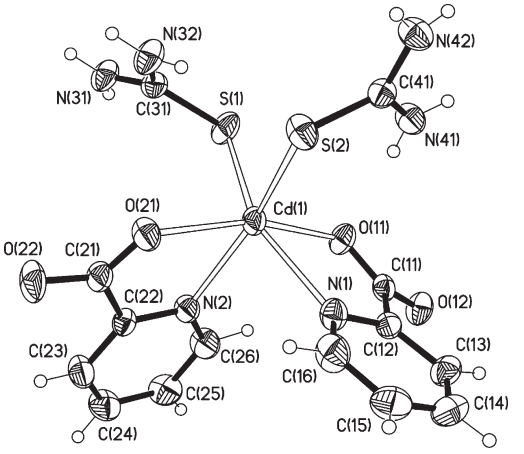

Figure 2. X-ray crystallographic structure of one of the two independent Cd(II) centers in **2a** with thermal ellipsoids at the 40% probability level.

Results and Discussion

Molecular Structures. The precursor complexes are readily prepared by mixing cadmium acetate dihydrate with the appropriate carboxylate ligand and either thiourea or thiosemicarbazide in hot water or hot aqueous ethanol. The ability to recrystallize the compounds is affected strongly by their solubilities. The dipicolinato complexes are moderately soluble in water; the picolinates display a higher solubility, whereas the salicylates are highly soluble. The complexes **1a**, **2a**, **2b**, **3a**, and **3b** crystallized readily, allowing their structures to be determined by single-crystal X-ray diffraction. Thermal ellipsoid plots of these molecules are shown in Figures 1−5.

Repeated attempts to obtain crystals from the reaction **1b**, however, were not successful and it is possible that the product exists as an equilibrium mixture in solution. An ESI-MS of the product designated as **1b** shows a dominant peak at 523.417 amu corresponding to a formulation of $Cd(sal)(ths)_3$ (see the Supporting Information, Figure S8A). In addition to this peak, several other peaks were seen. Those at 432.75 and 294.91 amu match $Cd(Hsal)(ths)_2$ (see Figure S8B in the Supporting Information) and $Cd(ths)_2$ (Figure S8C), respectively. Another major peak

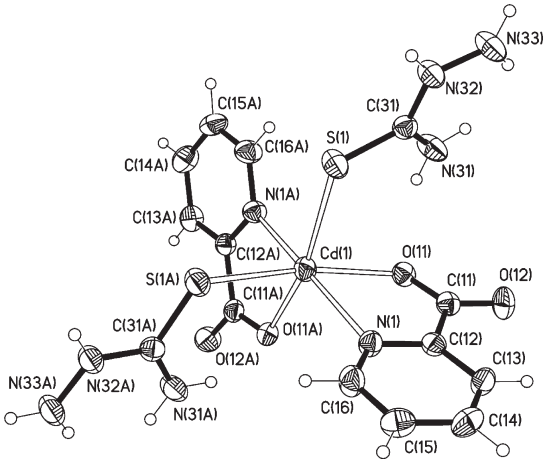

Figure 3. X-ray crystallographic structure of **2b** with thermal ellipsoids at the 40% probability level. The crystal lattice water molecules have been omitted.

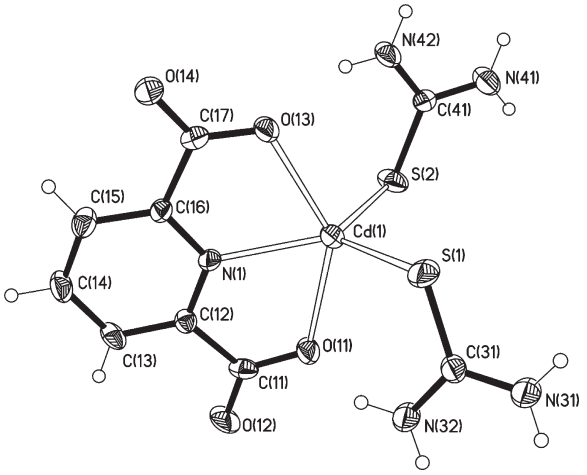

Figure 4. X-ray crystallographic structure of **3a** with thermal ellipsoids at the 40% probability level.

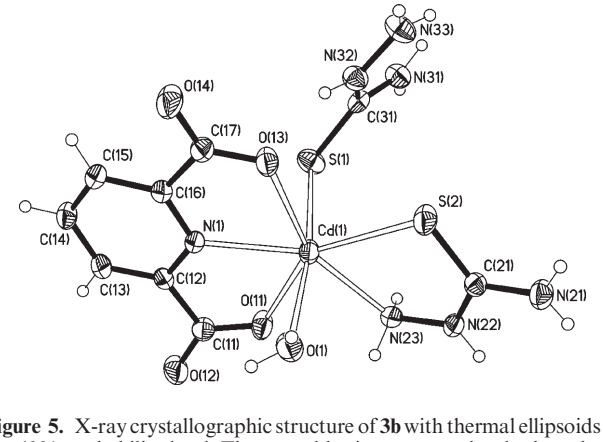

Figure 5. X-ray crystallographic structure of **3b** with thermal ellipsoids at the 40% probability level. The crystal lattice water molecules have been omitted.

at 385.83 amu corresponds to $Cd(Hsal)_2$ (see Figure S8D in the Supporting Information). Furthermore, there are some minor peaks at higher molecular masses that appear to be dimers of the lower molecular weight species. The likely formulations for molecules from this reaction are $Cd(sal)(ths)_x$ and $Cd(Hsal)_2(ths)_x$. All of the ions observed could be attributed to fragments of one or both of these species, but it is not possible to tell from these data if the product derives from a single complex or a mixture. Several equilibria are possible, including (1) Cd(sal) + H_2sal with $Cd(Hsal)_2$ and (2) either or both of these complexes with free ths. It should be noted that the ESI mass spectral data do confirm, however, that complexes with bound ths are present and that the product is not simply a mixture of either Cd(sal) or $Cd(Hsal)_2$ and isolated ths.

The salicylate ligand is known to bind to a single Cd(II) ion via the carboxylate functionality in either a monodentate or bidentate chelating fashion. In metal complexes salicylic acid can exhibit mono- or dideprotonation ($Hsal^-$ or sal^{2-}), with the latter case involving metal binding to the phenolic oxygen as well as the carboxylate. Only coordination to the carboxylate has been observed for Cd(II) complexes. This is the case for **1a**, where the bidentate chelating coordination mode is observed. One can view this bonding mode as existing along a continuum in which the metal is symmetrically bound to both carboxylate oxygen atoms to one in which only one oxygen can be considered bound. The binding can thus be somewhat or even highly asymmetric. This is seen in **1a** where the Cd−O distances are slightly different (2.468(19) Å vs 2.348(2) Å), whereas those to the other salicylate ligand are quite asymmetric (2.332(19) vs 2.8103(20) Å). A similar coordination mode is observed in the binuclear Cd(II) complex $[Cd(H_2O)_2(sal)_2]_2$, except that for this complex, dimerization is achieved by the coordination of one of the chelating carboxylate oxygens to an additional cadmium ion.[34] For that compound, the Cd−O bidentate−chelate distances are 2.3271 (24), 2.4338(23), and 2.3116(22) Å, whereas the bridging Cd−O distance is 2.5349(24) Å. The long Cd(1)−O(22) distance of 2.8103(20) Å (which is less than the sum of the listed van der Waals radii, Cd, 1.58 Å; O, 1.52 Å) indicates a weak, secondary bonding interaction.[35] If one considers all carboxylate oxygens to be bound, then the Cd(II) ion in **1a** can be thought of as possessing a highly distorted octahedral geometry with cis thiourea ligands. This is the most commonly found coordination geometry for Cd(II), although with thio-containing ligands a coordination number of 4 as well as 6 has been observed.[17,36−41] Alternatively, one could neglect the secondary Cd−O distance and describe the complex as penta-coordinate, but this is a much rarer occurrence. The Cd(II) ion in $Cd(th)_3SO_4$ is penta-coordinate.[36]

(34) Jian, F.; Xiao, H.; Sun, P.; Zhao, P. *Molecules* **2004**, *9*, 876.
(35) Bondi, A. *J. Phys. Chem.* **1964**, *68*, 441.
(36) Corao, E.; Baggio, S. *Inorg. Chim. Acta* **1969**, *3*, 617.
(37) Mautner, F. A.; Abu-Youssef, M. A. M.; Goher, M. A. S. *Polyhedron* **1996**, *16*, 235.
(38) Papatriantafyllopoulou, C.; Raptopoulou, C. P.; Terzis, A.; Janssens, J. F.; Manessi-Zoupa, E.; Perlepes, S. P.; Plakatouras, J. C. *Polyhedron* **2007**, *26*, 4053.
(39) Babb, J. E. V.; Burrows, A. D.; Harrington, R. W.; Mahon, M. F. *Polyhedron* **2003**, *22*, 673.
(40) Burrows, A. D.; Coleman, M. D.; Mahon, M. F. *Polyhedron* **1999**, *18*, 2665.
(41) Burrows, A. D.; Harrington, R. W.; Mahon, M. F.; Price, C. E. *J. Chem. Soc., Dalton Trans.* **2000**, 3845.

Compounds **2a** and **2b** both possess bidentate, chelating picolinate ligands, with one carboxylate oxygen atom and the pyridyl nitrogen bonded to the Cd(II) ion. Compound **2b** has crystallographically imposed 2-fold rotational symmetry. The metal ions in **2a** and **2b** also show distorted cis-octahedral coordination geometries. Interestingly, the picolinate ligands in **2a** adopt a trans arrangement of the carboxylate oxygen atom donors, resulting in an O(21)−Cd(1)−O(11) angle of 162.83(5)° while in complex **2b** the picolinate N donors are trans, giving rise to a N(1)−Cd(1)−N(1A) angle equal to 167.7(1)°. In the coordination polymers $[Cd(pic)(NCS)]_n$, and $[Cd_2(SO_4)(pic)_2(H_2O)_3]_n$ each picolinate ligand is attached to two Cd(II) ions.[44] One metal is bound as found in complexes **2a** and **2b**, while the other is chelated by sharing a carboxylate with another additional Cd(II) ion. For $[Cd(pic)(N_3)]_n$, the chelating mode as in **2a** and **2b** is also observed and each oxygen atom of the carboxylate ligand is attached to another Cd(II) ion; however, they are attached to different metals rather than forming a chelate structure.[37,38] The Cd−carboxylate bond distances for $[Cd(pic)(N_3)]_n$ vary from 2.247(5)−2.459(5) Å, whereas those for $[Cd(pic)(NCS)]_n$ lie in the range is 2.293(3)−2.453(3) Å.[43] The Cd−O bond distances in **2a** and **2b** are well within the same range (2.372(1) Å, 2.323(1) Å). The Cd−N (2.353(2), 2.383(2) Å) bond distances are also comparable to those observed in $[Cd(pic)(NCS)]_n$ and $[Cd(pic)(N_3)]_n$.

The only observed ligation mode for Cd with dipicolinate ligand is the tridentate mode in which the pyridyl nitrogen and one oxygen atom from each carboxylate unit are attached to the metal ion. Complex **3a** follows this observation. The penta-coordination is completed by two monodentate S-bound thiourea molecules. In contrast, one thiosemicarbazide ligand in **3b** is monodentate, while the second molecule acts as a chelating N,S ligand to form a five-membered ring. This bidentate coordination mode has also been observed in $[Fe(ths)_2SO_4]_n$, $[Cu(ths)Cl_2]$, $[Ni(ths)_2][C_6H_4\text{-}1,4\text{-}(CO_2)_2]$, $[Ni(ths)_2(H_2O)_2][trans\text{-}CO_2CH{=}CHCO_2]$, $[Zn(ths)_2(H_2O)_2][C_6H_4\text{-}1,4\text{-}(CO_2)_2]\cdot H_2O$, $[Et_2N][Co(ths)_3][Mo_8O_{26}]\cdot 4Me_2NCHO$ and $[Cd(ths)(HS)_2]_n$.[39−48] Water is also bound to the cadmium ion resulting in a seven-coordinate environment. This higher coordination number is likely responsible for the lengthening of the Cd−S bonds (Table 2).

In **3a** the Cd−O (2.398(3), 2.407(3) Å) and the Cd−N (2.264(3) Å) bonds are close to the range reported for Cd−O (2.2758(14)-2.3894(14) Å), Cd−N (2.2320(16), 2.2415(16) Å) in $(GH)_2[Cd(pydc)_2]$ (GH = guanidinium).[49] For **3b**, the increased coordination number and the water molecule within the coordination sphere causes an increase in the Cd−O and Cd−N bond distances. Tetracoordinate Cd(II) complexes generally exhibit shorter Cd−S bond distances (range 2.538−2.627 Å)[50] than those found in hexacoordinate complexes (range 2.638−2.761 Å).[51−53] By comparison, the Cd−S bond distance in pentacoordinate **3a** is one of the shortest known (2.518(2) Å), whereas the values seen for **1a**, **2a**, **2b**, and **3b** lie in the range consistent with other hexacoordinate complexes.

Table 2. Selected Bond Angles (deg) for 1a, 2a, 2b, 3a, and 3b

bond angle	1a	2a	2b	3a	3b
O(21)−Cd(1)−O(12)	94.68(8)				
O(21)−Cd(1)−O(11)	125.81(7)	162.83(5)	90.64(12)		
O(12)−Cd(1)−O(11)	53.87(7)				
O(21)−Cd(1)−S(1)	97.99(5)	104.42(5)	165.26(7)		
O(12)−Cd(1)−S(1)	97.39(6)				
O(11)−Cd(1)−S(1)	125.79(5)	80.14(5)	93.81(7)	101.67(9)	90.27(7)
O(21)−Cd(1)−S(2)	108.22(6)	86.30(4)	86.30(4)		
O(12)−Cd(1)−S(2)	149.90(6)				
O(11)−Cd(1)−S(2)	96.28(5)	109.67(4)	165.47(16)	98.91(8)	143.24(6)
S(1)−Cd(1)−S(2)	98.43(3)	98.20(2)	85.40(5)	113.68(5)	98.05(4)
N(1)−Cd(1)−O(11)		69.68(6)	70.60(11)	70.0(1)	
N(1)−Cd(1)−O(13)				70.4(1)	67.64(8)
O(11)−Cd(1)−O(13)				140.41(1)	
N(1)−Cd(1)−S(2)		89.40(5)	94.76(9)	124.3(1)	146.25(6)
O(13)−Cd(1)−S(2)				101.82(8)	79.20(5)
N(1)−Cd(1)−S(1)		149.67(4)	94.44(9)	122.0(1)	87.68(7)
O(13)−Cd(1)−S(1)				100.34(9)	88.83(6)
N(1)−Cd(1)−N(23)					139.71(8)
N(1)−Cd(1)−O(1)					84.69(9)
N(23)−Cd(1)−O(1)					87.54(9)
N(23)−Cd(1)−O(11)					70.45(8)
O(1)−Cd(1)−O(11)					82.85(9)
N(23)−Cd(1)−O(13)					152.33(8)
O(1)−Cd(1)−O(13)					92.40(8)
N(23)−Cd(1)−S(2)					73.14(6)
O(1)−Cd(1)−S(2)					90.80(7)
N(23)−Cd(1)−S(1)					95.43(7)
O(1)−Cd(1)−S(1)					171.14(6)
O(21)−Cd(1)−N(2)		71.27(5)	70.60(11)		
N(2)−Cd(1)−O(11)		91.85(5)	100.30(11)		
O(21)−Cd(1)−N(1)		105.34(6)	100.30(11)		
N(2)−Cd(1)−N(1)		87.25(6)	167.47(16)		
N(2)−Cd(1)−S(1)		96.89(4)	96.89(4)		
N(2)−Cd(1)−S(2)		155.49(4)	94.44(9)		

The crystal packing of the complexes (Figures S25−S29 in the Supporting Information) reveal that hydrogen bonding and/or $\pi-\pi$ stacking interactions play an important role in the supramolecular association of the monomeric units. Intermolecular hydrogen bonding often takes place in between the carboxyl oxygen and the amine groups on the thiourea or thiosemicarbazide ligands. There does not appear to be intermolecular N−H···O

(42) Burrows, A. D.; Harrington, R. W.; Mahon, M. F.; Teat, S. *J. Cryst. Growth* **2004**, *4*, 813.
(43) Burrows, A. D.; Menzer, S.; Mingos, D. M. P.; White, A. J. P.; Williams, D. J. *J. Chem. Soc., Dalton Trans.* **1997**, 4237.
(44) Chattopadhyay, D.; Majumdar, S. K.; Lowe, P.; Schwalbe, C. H.; Chattopadhyay, S. K.; Ghosh, S. *J. Chem. Soc., Dalton Trans.* **1991**, 2121.
(45) Burrows, A. D.; Mingos, D. M. P.; White, A. J. P.; Williams, D. J. *Chem. Commun.* **1996**, 97.
(46) Dunaj-Jurco, M.; Kozisek, J.; Cagan, P.; Melnik, M.; Sramko, T. *J. Cryst. Spectrosc.* **1992**, *22*, 51.
(47) Li, S.-L.; Wu, J.-Y.; Tian, Y.-P.; Tao, X.-T.; Jiang, M.-H.; Fun, H.-K. *Chem. Lett.* **2005**, *34*, 1186.
(48) Zhang, H.; Niu, S.; Yang, G.; Nie, F.; Li, S. *Transition Met. Chem.* **1994**, *19*, 498.
(49) Moghimi, A.; Sheshmani, S.; Shokrollahi, A.; Aghabozorg, H.; Shamsipur, M.; Kickelbick, G.; Aragoni, M. C.; Lippolis, V. *Z. Anorg. Allg. Chem.* **2004**, *630*, 617.
(50) Gray, I. P.; Slawin, A. M. Z.; Woollins, J. D. *J. Chem. Soc., Dalton Trans.* **2004**, 2477.
(51) Bigoli, F.; Braibanti, A.; Manotti Lanfredi, A. M.; Tiripicchio, A.; Tiripicchio Camellini, M. *Inorg. Chim. Acta* **1971**, *5*, 392.
(52) Castro, R.; Garcia-Vazquez, J. A.; Romero, J.; Sousa, A.; Pritchard, R.; McAuliffe, C. A. *J. Chem. Soc., Dalton Trans.* **1994**, 1115.
(53) Moloto, N.; Revaprasadu, N.; Moloto, M. J.; O'Brien, P.; Helliwell, M. *Polyhedron* **2007**, *26*, 3947.

Table 3. Summary and Comparison of Nanoparticle Shapes from Single Source Precursors

precursor	conditions	shape	ref
$Cd(ths)_2Cl_2$	TOPO, 280 °C	nanorods	13
$Cd\{S_2C(NHR)\}_2$; R = Et, Bu, C_6H_{13}, $C_{12}H_{25}$	hexadecylamine, 200 °C	mixture of nanorods, bent nanorods	12
$Cd\{S_2CNEt_2\}_2$	pyridine, Et_2NH, 120 °C	spherical aggregates	64
$Cd\{S_2CNEt_2\}_2$	en, $H_2NNH_2 \cdot H_2O$, 120 °C	nanorods, multiarm nanorods	64
$Cd\{n\text{-}C_8H_{17}O)_2PS_2\}_2$	oleyl amine, 160 °C	quantum dots	65
1a, **1b**, **2a**, **2b**, **3a**, **3b**	hydrothermal, CTAB	gypsum rose	this work
1a, **1b**, **2a**, **2b**, **3a**, **3b**	en + hexadecylamine	nanorods	this work
1a, **1b**, **2a**, **2b**, **3a**, **3b**	oleylamine	spherical particles	this work
1a, **1b**	oleylamine, HCl	ellipsoidal particles, short nanorods	this work
1a, **1b**	oleylamine, TOPO, HCl	ellipsoidal particles	this work
1a, **1b**	oleylamine, TOP	mixture of nanorods and multipods	this work
2a, **2b**, **3a**, **3b**	oleylamine, TOP	nanorods	this work

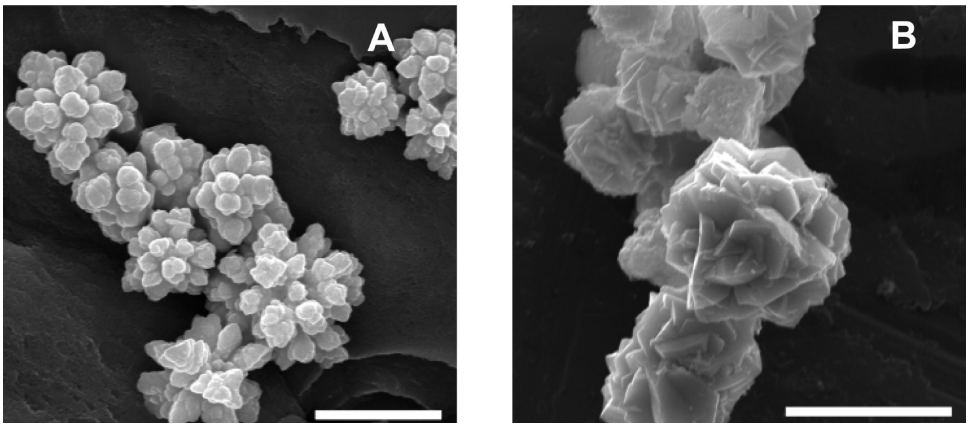

Figure 6. SEM images of (a) the flowerlike CdS particles from **1a**, and (b) semispherical aggregates of CdS from **2b**. (scale bars = 2 μm).

hydrogen bonding in **1a**, where all of the N···O separations are very long (> 4.7498(35) Å). For comparison, the O−H···O hydrogen bond distances in $[Cd(H_2O)_2(sal)_2]_2$ lie between 2.5222 and 3.0104 Å, whereas in the coordination polymer $[Cd_2(SO_4)(pic)_2(H_2O)_3]_n \cdot nH_2O$, they vary between 2.723(15) and 2.934(16) Å. In **2a** and **2b**, the intermolecular N−H···O hydrogen bond distances were found to vary in between 2.8545(27) and 4.6019(51) Å. For **3a** and **3b**, the N−H···O hydrogen bonding distances were found to lie between 2.9618(31) and 4.3147(57), which was reasonably comparable to $(GH)_2[Cd(pydc)_2]$ (GH = guanidinium) in which the N−H···O hydrogen bonding distances lie between 2.752 and 3.014 Å.

Synthesis of CdS Nanoparticles. The decomposition reactions were carried out using both aqueous and organic solvents. A variety of different shapes were obtained depending upon conditions. Table 3 gives a comparison of the types of structures for our studies as well as those reported for other single-source precursor decompositions. For all of the decomposition reactions, the picolinate and salicylate precursors behaved differently as compared to the dipicolinates. It can be assumed that dipicolinate, being a tridentate ligand binds to Cd(II) more strongly, and under the applied decomposition conditions would hydrolyze at a different rate. It was found that the dipicolinate precursors gave mostly micrometer sized particles of irregular shape under aqueous conditions while agglomeration of very small round particles was observed when they were decomposed in long chain organic amines. Hence more attention was given to studying the salicylate and picolinate precursors that gave more desirable decomposition results.

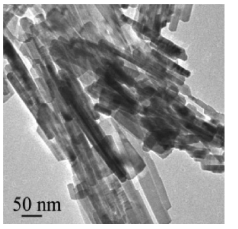

Figure 7. TEM image of the rodlike CdS nanostructures generated from the decomposition of **1a** in ethylenediamine.

The presence of carboxylic acid and hydroxyl groups in the precursor structures assist their solubility in aqueous solutions, so initial decomposition attempts were carried out under hydrothermal conditions in the presence of CTAB. Figure 6 shows the results obtained from precursors **1a** and **2b**. This procedure yielded flowerlike particles, from several hundred nm to several μm in diameter for **1b**, while for **2b** the particles were 2−4 μm in diameter, with the leaflets being about 100−250 nm thick with lengths and widths varying up to micrometer size. Precursors **1b** and **2a** gave similar results with a wider distribution of sizes, whereas **3a** and **3b** gave mostly round micrometer-sized particles (see the Supporting Information for decomposition results from **3a** using CTAB). The semispherical aggregates of CdS formed from the

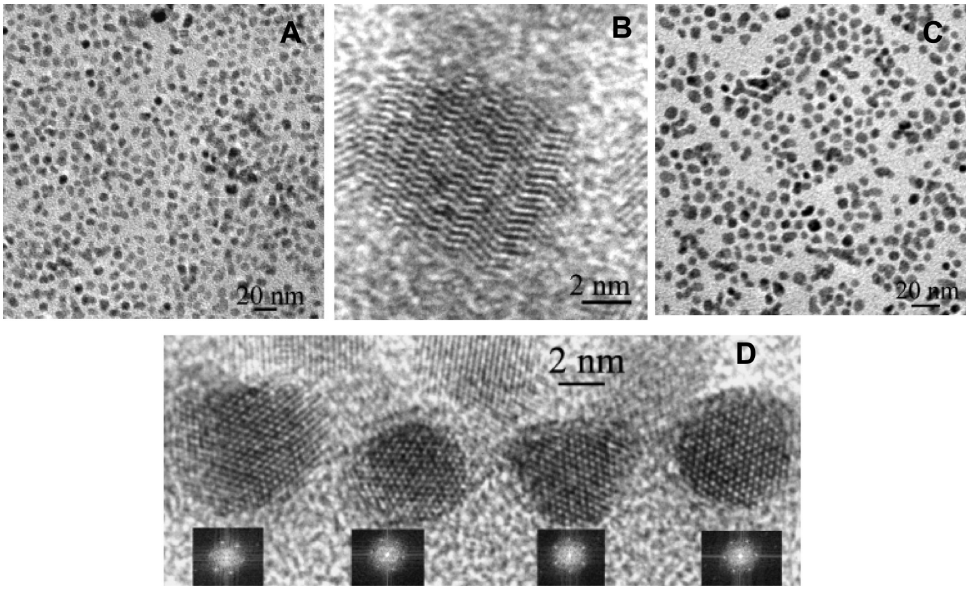

Figure 8. (A) Conventional TEM image of spherical CdS nanoparticles synthesized with oleylamine from precursor **1a**. (B) HR TEM image of one of the particles shown in A reveals polysynthetic twins in the hexagonal phase. (C) Conventional TEM image of spherical CdS nanoparticles synthesized with oleylamine from precursor **2b**. (D) HR TEM images and FFT of four NPs shown in C confirm all four of them have $[001]_{hex}$ zone axis orientation but are rotated relative to each other along this zone axis.

picolinate and dipicolinate precursors have the same morphology as the formation known as the desert-rose or gypsum rosette.[55] The formation of such crystals was explained by the uneven deposition rates during quick crystallization from supersaturated solutions, resulting in anisotropic shapes. The XRPD pattern of all the hydrothermal products show sharp peaks corresponding to stable hexagonal CdS (greenockite, JCPDS #01−077−2306). The EDS data confirmed the presence of both Cd and S in the particles in a 1:1 ratio (see the Supporting Information for characteristic EDS of decomposition product from precursor **1a**). In the thermogravimetric analysis (see the Supporting Information for characteristic TGA curve of precursor **2b**) of the precursors, a single large decomposition step is observed that roughly corresponds to the weight loss due to the loss of the carboxylate ligand. Previous studies have shown that the organic byproducts of the decomposition may cap the surfaces of growing nanoparticles affecting their shapes and sizes. Other parameters such as temperature, surfactant, concentration of reagent, injection procedure, growth time, and presence of structure-directing coordinating solvents also influence the growth of cadmium chalcogenide nanocrystals.[11,54]

Decomposition of the precursors was also examined in several different amine solvents: ethylenediamine, hexadecylamine, trioctylamine, and oleylamine. Amines are known to be good solvents for allowing control over the morphology of cadmium chalcogenide NP's.[56,57] The reaction temperatures used were either 120 or 175 °C, and the reaction time was varied from 2 to 16 h. The best shaped NPs were obtained when the decompositions were carried out in a mixture of ethylenediamine and hexadecylamine at 175 °C for 2 h. Rodlike CdS nanocrystals were formed as the final products from all six precursors. The representative TEM image shown in Figure 7 is obtained from precursor **1a** decomposed in ethylenediamine. Interestingly, the rodlike CdS nanocrystals were found by XRPD to be predominantly a metastable orthorhombic phase. The hexagonal form was also found to be present in smaller extent. The low decomposition temperature of single-source precursors may be responsible for allowing access to the metastable phase. It has been shown in literature previously that use of nickel and zinc diethyldithiocarbamates gave rise to metastable crystal modifications of Ni_3S_4 and ZnS.[9,10]

When using oleylamine as a surfactant, the products obtained by decomposition of the complexes at 120 °C are in the form of spherical particles. The morphology of the decomposition products from precursor **1a** and **2b** are shown in Figure 8. Here the XRPD matches with a metastable orthorhombic phase, some of the expected hexagonal phase were also detected. Polycrystalline SAED patterns from these samples confirmed the presence of both phases. The difference between the XRPD and TEM results is that the XRPD analysis shows predominantly the orthorhombic phase while in the TEM study, the hexagonal phase is dominant. This can be explained by the metastability of the orthorhombic phase, which is transformed to the hexagonal phase over a short period of time. The HR TEM images of some NPs show the presence of a high density of planar defects (particularly twins) that are likely formed during the NPs' growth. Twinning generally produces an aggregate symmetry higher than that of each of the individual components because the twinning planes or axes are

(54) Li, Y.; Li, X.; Yang, C.; Li, Y. *J. Mater. Chem.* **2003**, *13*, 2641.
(55) Sunagawa, I., *Crystals Growth, Morphology and Perfection*; Cambridge University Press: Cambridge, U.K., 2005.
(56) Chen, F.; Zhou, R.; Yang, L.; Liu, N.; Wang, M.; Chen, H. *J. Phys. Chem. C* **2008**, *112*, 1001.
(57) Yao, W.-T.; Yu, S.-H.; Liu, S.-J.; Chen, J.-P.; Liu, X.-M.; Li, F.-Q. *J. Phys. Chem. B* **2006**, *110*, 11704.

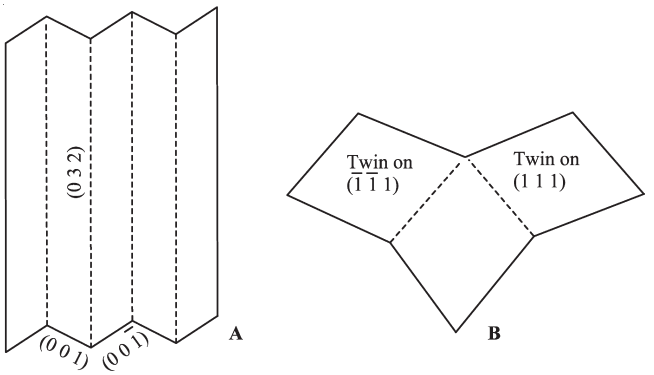

Figure 9. (A) Polysynthetic and (B) multiplet twinning. (A) represents the hexagonal phase polysynthetically twinned on (032). The zone axis orientation is [100]. (B) is a section of fcc phase (twinned on the symmetry related planes (111) and ($\bar{1}$11) so as to become a triplet. The zone axis orientation is [011]. See reference 63.

added symmetry elements. Twin formation could also minimize internal crystal energy. The HR TEM image in Figure 8B reveals polysynthetic twins (see Figure 9A). The hexagonal phase particle has a [100] zone axis orientation. Matrix and twin planes are (001) and (00$\bar{1}$), respectively. The twinning plane is (032). Figure 8D shows that there are also some NPs that are almost defect free. For the four NPs observed here FFT confirms that all have the same [001] zone axis orientation (hexagonal phase) but are rotated relative to each other along this zone axis. The distances between them are reasonably uniform and small enough that they could be considered as grain boundaries, taking into account the surfactant layer around them. In our TEM studies of CdS as well as many other materials [e.g., Bi_2S_3, PbS, MnO_x, Fe_xO, $Fe_{1-y}Mn_yO$, In_2O_3, Fe_2P] we have never observed NPs totally free of defects (point, linear, planar) even when their size is as small as 2−4 nm. Also, we have never observed NP growth via oriented attachment in these materials.[4,58−62]

When the salicylate precursors were decomposed using oleylamine in the presence of a very small amount of concentrated HCl, the decomposition products tended to be more ellipsoidal or short rods (see Supporting Information for results from precursor **1a**). When the salicylate precursors **1a** and **1b** were decomposed using a mixed surfactant of oleylamine and TOPO in the presence of small amount of HCl ellipsoidal particles were obtained. Figure 10 shows the results from precursor **1b**, all other precursors gave mostly small round nanoparticles under same condition. The XRPD and polycrystalline SAED patterns of these nanoparticles match the hexagonal

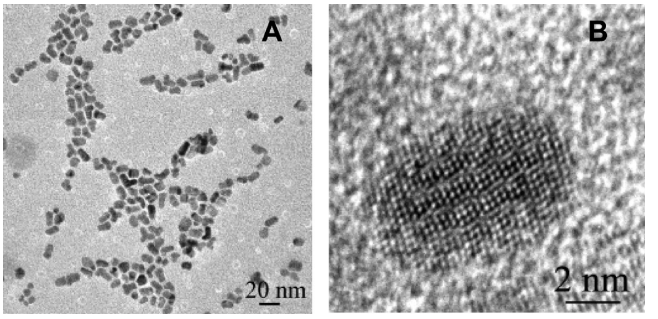

Figure 10. (A) Conventional and (B) HR TEM images of ellipsoidal CdS particles synthesized in oleylamine with added TOPO and HCl from precursor **1b**.

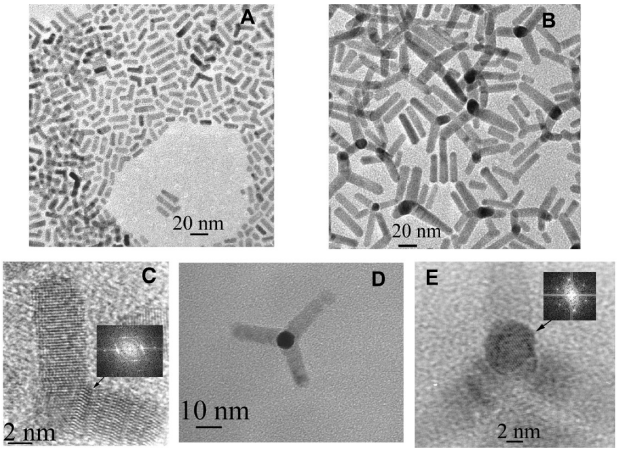

Figure 11. Conventional and HR TEM images of multibranched nanoparticles synthesized from precursor **1b** in oleyl amine in the presence of TOP and HCl. (A) Mixture of rods and bipods generated without using any dodecanethiol in the surfactant. (B) Mixture of rods, bipods, tripods, and tetrapods generated in the presence of a small amount of dodecanethiol. (C) HR TEM image one of the bipod structures shown in A, FFT is obtained from the core of the particle. (D) Enlarged image of one of the tetrapod structures from B. (E) HR TEM image of the tetrapod and FFT obtained from its central part.

phase. The HR TEM image of a single NP (Figure 10B) revealed a high density of both linear and planar defects.

When the decomposition of the salicylate precursors **1a** and **1b** was performed in a mixture of oleylamine and TOP (Figure 11 A and C), a mixture of nanorods and multipods formed. With all other precursors (**2a**, **2b**, **3a**, **3b**), very little branching was observed with mostly small rod shaped nanoparticles. It was found that using precursor **1b** in the presence of a small amount of dodecanethiol (DDT) more tripods and tetrapods were generated, and the branches on the multipods grew as long as 60 nm (Figure 11B). Addition of phosphonic acids has been shown to favor twinning and initiate the branching.[22] This is possible in our system since some n-trioctylphosphine may decompose to a phosphonic acid under the reaction conditions. The XRPD and polycrystalline SAED patterns of the multibranched CdS particles given in Figure 11 show the presence of both fcc and hexagonal phases; however, it appears that the hexagonal phase is dominant (see Figure S14 in the Supporting Information). The FFT simulated from the particle shown in Figure 11C shows that the core has a ⟨011⟩ orientation for

(58) Hofmann, C.; Rusakova, I.; Ould-Ely, T.; Prieto-Centurion, D.; Hartman, K. B.; Kelly, A. T.; Luttge, A.; Whitmire, K. H. *Adv. Funct. Mater.* **2008**, *18*, 1661.
(59) Mandal, T.; Stavila, V.; Ould-Ely, T.; Rusakova, I.; Whitmire, K. H. Manuscript in preparation.
(60) Rusakova, I.; Ould-Ely, T.; Hofmann, C.; Prieto-Centurion, D.; Levin, C. S.; Halas, N. J.; Luettge, A.; Whitmire, K. H. *Chem. Mater.* **2007**, *19*, 1369.
(61) Stavila, V.; Rusakova, I.; Whitmire, K. H. *Chem. Mater.* **2009**, DOI: 10.1021/cm902229x.
(62) Ould-Ely, T.; Prieto-Centurion, D.; Stavila, V.; Rusakova, I., Whitmire, K. H. Manuscript in preparation.

the fcc phase. Multiplet twinning (Figure 9B) on the planes would initiate triplet formation. The generation of stacking faults that initiate the atom sequence for the hexagonal phase are observed in the HR TEM image. Two hexagonal branches continue the NP growth. Other planar defects present in the growing branches are polysynthetic twins similar to those that were observed in the NP shown in Figure 8B. The TEM images in Figure 11C−E of the tripods and tetrapods can be explained similarly to the formation of the particles with only two branches. Multiplet twinning could result in formation of more than two branches. The FFT obtained from the central part of the tetrapod (Figure 11E) shows a hexagon that can be indexed to the ⟨111⟩ zone axis for the cubic core and [001] zone axis for the fourth hexagonal branch that is aligned with the direction of view.

There are different schools of thought on the generation of multipod-based nanostructures. One theory believes these structures originate from polytypism or coexistence of two crystal phases on different parts of a crystal structure. In polytypic crystals two different crystal domains share a common facet; researchers have shown for CdTe and CdSe tetrapods that the core adopts the cubic phase whereas the arms grow in the hexagonal phase.[19] It is further believed that the growth of these branched nanostructures depends on the relatively small energy difference between the two crystalline phases. The other school of thought suggests that the presence of a multiple twin nucleus with four fast and four slow growing facets is responsible for the branched nanostructures.[22] Our HR TEM studies suggest that polysynthetic twinning and multiplets are responsible for the generation of the branched nanostructures. To some extent, these two views are simply extremes of the same process where the dominant role is played by planar defects. In one case, stacking faults lead to a clean transition from one phase domain to another (core versus arm), whereas in the others, various types of twinning lead to growth of NPs.

Conclusions

Aromatic carboxylate complexes of Cd(II) form stable adducts with thiourea or thiosemicarbazide. These compounds are easy to synthesize, stable under ambient conditions, and possess good solubility in common organic solvents and water. They can be used as molecular precursors for CdS semiconducting NPs in either aqueous or nonaqueous solvents. From the accumulated data, it is clear that nanoparticle shapes are highly sensitive to the solvent/surfactant system employed as well as to the ligands attached to the metal center. In cases where the ligands can bind to one or more of the growing nanoparticle surfaces but not all, asymmetry in the structures results. The systems, however, are still too complex to make detailed predictions about what shape(s) will arise from a given set of ligands, solvents/surfactants and other additives a priori. In our decomposition reactions, the more uniform particle shapes were obtained from salicylate and picolinate precursors. Long chain organic amines were found to be the most effective surfactant giving small nanoparticles of spherical to ellipsoidal shape. A combination of oleylamine and TOP were found to give branched nanoparticles from salicylate precursors. Aqueous reaction conditions yielded largely micrometer-sized particles, suggesting slower precipitation from aqueous solution than from predominantly organic solvent systems. Additionally, using the mild decomposition conditions, metastable orthorhombic CdS can be accessed that has not been previously reported from single-source precursor methods.

The data obtained in these studies are consistent with the branching in nanocrystals arising from multiplet and polysynthetic twinning. An important aspect of this finding is that an arm in a polypodal structure is not necessarily a single type of phase structure (e.g., fcc or hexagonal) but these arms can also exhibit polysynthetic twinning and maintain a linear geometry as seen in Figure 11C. This appears to result when trioctylphosphine is used as an additive in the decomposition reactions.

Acknowledgment. We gratefully acknowledge financial support from Welch Foundation (C-0976), the National Science Foundation (E-0411679), and the CRDF for a research grant (Award MTFP-1015).

Supporting Information Available: CIF files giving crystallographic data for **1a**, **2a**, **2b**, **3a**, and **3b**; packing structures of the crystals showing hydrogen bonding, XRPD of decomposition product, optical and photoluminescence spectra, ^{13}C NMR, IR spectra with peak assignments, and TGA for the complexes (PDF). This material is available free of charge via the Internet at http://pubs.acs.org.

(63) McKie,D.; McKie, C., *Crystalline Solids* Thomas Nelson and Sons Ltd.: Nashville, TN, 1974.
(64) Zhang, Y. C.; Wang, G. Y.; Hu, X. Y. *J. Alloys Compd.* **2007**, *437*, 47.
(65) Lou, W.; Chen, M.; Wang, X.; Liu, W. *Mater. Lett.* **2007**, *61*, 3612.